REGULAR PAPER

Sensing of refractive index by using guided mode resonance 1D TiO$_2$ grating at visible wavelength under normal incidence

Khizzra Aslam[1] · Nouraiz Mushtaq[2] · Guoguo Kang[1] · Zhao Luo[1]

Abstract

The effects of guided mode resonance (GMR) are largely used in optical communications because of its accurate line width and good capability. Specially study of titanium dioxide (TiO$_2$) gratings on glass substrate exhibit very low losses and can have excellent diffraction abilities along annihilation ratios. In this study a significant refractive index sensing by using the grating mode resonance in a simple 1D TiO$_2$ dielectric gratings. The resonant peak produced through structural asymmetry chosen as sensing probe. The narrow line width of resonance peak boosts the figure of merit. We presented excellent sensing results can be continued over a broadband range in visible region with comparatively large deviations in grating depth and period. Simulation shows the sensor possessing RI sensitivities of 352.57 nm/RIU and FOMs of 1176 for resonant peak. This GMR-based dielectric sensor device which is easy for manufacture is anticipated to show great declaration for achieving broadband refractive index sensors with better performance.

1 Introduction

The effect of guided mode resonance (GMR) has obtained large interests in different applications, like optical filters, optical switches and biosensors [1–9]. The benefits can mainly ascribe to their smooth structure, great efficiency, and tunable fine line width [10]. A distinctive GMR structure has sub-wavelength gratings with high refractive-index dielectric layer [11]. The brightness of incident light which satisfies the state match point can advance the guided modes (GM). Collectively, the light at the GM's may be continually extracted over the periodic modulation of grating, and it interferes with the destructively conduction of light and constructively reflection of light, making in a resonant peak which indicate good efficiency at a suitable wavelength. Sub wavelength gratings can help split guided modes dominant to transmission descend in diffraction spectrum and acute resonant peaks of reflection, which is known as the guided-mode resonance (GMR) [8]. For certain factors of the grating waveguide configuration, the position of the fine peak

in the reflection band depends on the refractive index (RI), grating parameter and incident angle of the medium. GMR wavelength has been associated to the refractive index of the surroundings, for that the GMR-based apparatus can be used as refractive index sensor with good result because of its very small line width as well as sensitivity to the medium [12–14]. In the use of refractive index sensors, the sensitivity of RI is usually defined in means of the alteration in peak location per refractive index unit (RIU) that is an important factor to calculate sensing capability. One more key parameter defining the sensing application is the figure of merit (FOM). A good FOM relates with RI sensor for its extraordinary sensing ability that may improve through enlarging its sensitivity and subdue its resonance line width. Actually, the FOM rises with accumulative sensitivity and reducing FWHM. Basically, a sensor having high FOM is capable to sense the lower RI variations, so giving great proficient sensing capacity.

By using SPP or LSP supported with noble metal for sensor is fascinating great consideration because of its good sensitivity to the medium of the stimulated interfaces. [15]. There are also several types of structures have been reported by using SSP- based plasmonic waveguides in literature like metal films, metal nanoparticle chains, metal grooves, MIM gaps, metal–insulator–metal (MIM) slabs, metal wedges, metal strips, metal wedges, all optical compact D flip-flops, 1-D waveguide sensors, Hybrid Nanostructures, gas sensor

✉ Khizzra Aslam
  khizzraa@yahoo.com

1 School of Optics and Photonics, Beijing Institute of Technology, Beijing 100081, China

2 Schoolof Material Science and Engineering, Zhejiang Sci-Tech University, Hangzhou, China

and hybrid Bragg waveguide have been recommended. The graphene-based plasmonic waveguides and strips have been also deliberated in different devices because of the distinctive property of graphene such as flexibility, high limitation, tunability, great carrier movement, transparency, mechanical toughness, and truncated damage at terahertz frequencies [16–20]. Amongst them one-dimensional structures are significant which have fascinated increasing attentions for flexible and compact applications in optical sensors.

In these years, several attempts have dedicated to overturn the resonance line width to enhance the figure of merit in plasmonic sensors with the use of Fano resonances ascending from the combination between wide super-radiant and thin sub-radiant modes [19–22] or arranging metal nanoparticles into 1 or 2D groups [23–25]. However the full width half maximum of this metal-based RI sensor till passes 3 nm because of the ohmic deficiency in the metal. An efficient way for decreasing the resonance line width is to employ dielectric photosensitive device lacking any metal element, therefore evading ohmic deficiency. RI biosensors are defined through a large sensitivity of the resonance spectral point to the RI deviations.

Improving the sensitivity of a sensor is the main attention of dedication in the literature. Different types of optical sensor have also been studied in literature for obtaining high sensitivity. Photonic crystals and their structure by using Graphene-Al_2O_3 [26] has been used recently to design optical sensor and for guiding the optical wave transmission by using waveguides. It also offer influential means for adjusting the interactions among matter and light due to their good quality factor as well as narrow mode volume, which are stimulated large interests on the area with quantum information dispensation, optofluidics, nonlinear optics and optical trappings. Photonic crystal nanobeam (PCN) sensors exhibits so much merits achieving an excellent quality factor. Though, the relations of spatial distribution, optical dispersion and symmetries are still scarcely tuned when the configurational parameters are permanent, it means the resonant property of modulator centered on PCN cannot be manageable after fabrication. Literature studies propose diverse and simple structures with enhanced optical as well as fundamental features in order to increase the electromagnetic field constraint in the sensing region and after that advance the sensing capability [27–29].

Here, we introduce a RI sensor based on the dielectric GMR by good FOM above 1100, which useful with the smooth one dimensional grating which backs very narrow GMR line width till 0.25 nm. However, the simplicity of revealing method go with the moderate quality (Q) factors (generally limited in a range of 100∼300) associated to the sensitivity method that usually can attain large-Q factors to 104 [30, 31]. A large-Q factor configuration effects in the capability to measure low resonant wavelength changes with greater precision, thus decreasing limits of detection (LOD) [32]. Over the past few years, major research efforts are devoted to succeed large Q GMR devices. We additionally investigate the effect of geometric constraints like period and grating depth on the results of the suggested refractive index sensor, through changing geometric restrictions together, we may attain RI sensing with good result above a broadband array in close infrared area.

From above mentioned properties, GMR configurations can be utilized in several diverse fields, like optoelectronics, biosensing and optical communications etc. The major part of the research so far pact through thin dielectric grating combined with the thin dielectric PWL, and just limited deals with thick dielectric grating, simply without planar wave guide layer, mostly not as a filter or sensor. The importance of thick gratings, and predominantly those with a large refractive index difference, has amplified in the previous era [33–38] because of the improved attention in resonant modes, like cavity as well as Fano resonances, and moreover because of the case that the nanosynthesis of gratings through large aspect ratios becomes achievable. In this work, we focus on the design of GMR configuration using thick grating without PWL for RI sensing application and the dependency of the sensor based on different of parameters. This GMR-based dielectric sensing device which is easy to fabricate is estimated to hold good potential for understanding broadband RI sensor with excellent performance as well as compactness.

2 Simulation work

Two-dimensional simulations were performed with Lumerical FDTD, a commercial electromagnetics software package. A normal incidence, broadband plane wave source was assumed with polarization along the grating direction. Periodic and PML boundary conditions were used on the X and Y boundaries. As the system under consideration is large, but it shows translational symmetry on smaller length scales within it, the external boundaries of the model have been set to periodic boundary conditions (PBCs). Perfectly similar layers were used for the basic boundaries as the absorbing region to compete for infinite space. Palik data had been used for SiO_2 in simulation. A refined override mesh of 2 nm was tested over the entire simulation area For optical simulations by changing grating parameters are shown in further figures generated using Lumerical FDTD. The structure had been modeled for a two-dimensional finite TiO_2 ($n=2.44$) grating ($w=343$ nm, $h=612$ nm, $N=3$, and $P=500$ nm) inserted in SiO_2 ($n=1.45$) as shown in Fig. 1a, the mesh of 2 nm was used in every direction as well as the structure modes determined at 514 nm wavelength along the xy direction. The spatial cell size and the simulation interval time
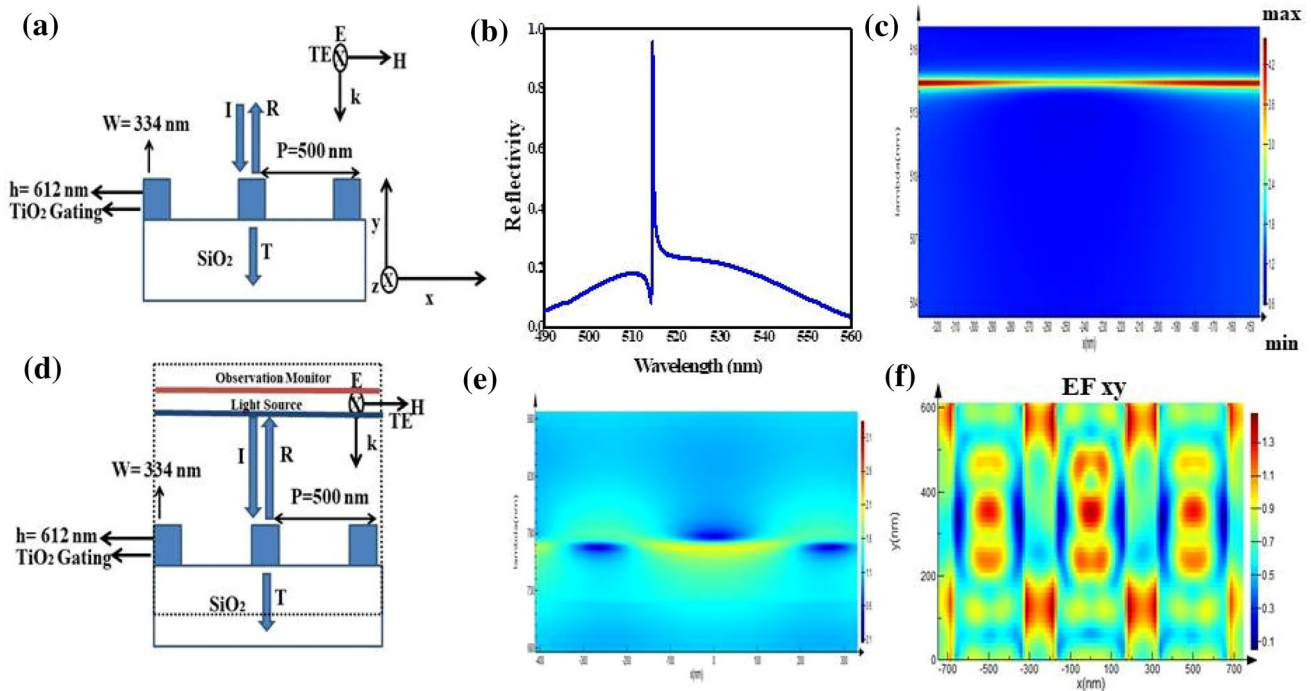
Fig. 1 **a** Schematic diagram of 1D TiO$_2$ RI sensor with grating height = 612 nm, period = 500 nm and width = 343 nm. The refractive indices of the grating and background environment are ng = 2.44 and nc = 1.0, respectively. The light illuminated on the nanostructure is TE polarized with incident angle θ = 0 **b** Simulated reflected spectra of TiO$_2$ grating **c** Electric field enhancement at resonant wavelength along xy-axis **d** Cross sectional view of FDTD calculation model(**e, f** Electric field distribution at two different wavelength along 2D z-normal direction

are 2 × 2 nm^2 and 4.7 × 10^{-18} s, respectively, and these values are sufficient to assure the convergence of the simulation.

We have simulated the designed structure by using normal incident TE illumination (electric field along the z-direction and magnetic field in the xy plane), as shown in Fig. 1a. TiO$_2$ grating are periodic in the x-direction (with a period lesser than the excitation wavelength in order to obtain the only zero-order reflection), fixed in the z-direction and predetermined in the y-direction. We also presumed the infinite lengths of each configuration parts in the z-direction. These propositions are acceptable as the definite structure for z-direction is greater than the stimulated plane wavelength. The vector of the incident electric field might be analogous (TE) to the grating positions. The light source generally enters the configuration of surface and moves from the higher part of the TiO$_2$ grating as well as enters into substrate which proves that the reflection resonant modes comparable to the normal GMR, due to the layer of grating itself can work like a waveguide.. The simulated refection spectra are shown in Fig. 1b as a function of the incident wavelength. The GMR excitation in the xy-direction can be shown by the electric field enhancement at resonant wavelength given Fig. 1c. The simulation region was enclosed by dotted lines shown in Fig. 1d. The dotted line demonstrates the boundary conditions in this simulation. The reflection

spectrum and electric field enhancement of the structure was designed by the reflection monitor/observation monitor. Two cases have also been observed for electric field distribution along 2D Z-normal direction by using larger source span, one at resonant wavelength and other is at 720 nm. There is no resonant produce for 720 nm, which shown in Fig. 1e. The electric field distribution at resonant wavelength 514 nm given Fig. 1f, which obviously determines the propagating features of GMR guided by the periodic dielectric slits.. We will observe in further discussion that such a narrow GMR peak plays a significant part in understanding high-performance refractive index sensing.

3 Results and discussion

To understand the strength of sensing properties of our GMR-based device, we changed the RI of background environment from 1.0 to 1.1 with minor variations of n = 0.01 for resonant peak. Background RI varies from 1 to 1.01 while keeping Background temperature of our GMR structure at 300 k. As the RI changes with minor variations, peak shows red-shift, as shown in Fig. 2a.

The peak position (blue symbols) were shown in Fig. 2b, which shows the peak wavelength of our GMR-Structure
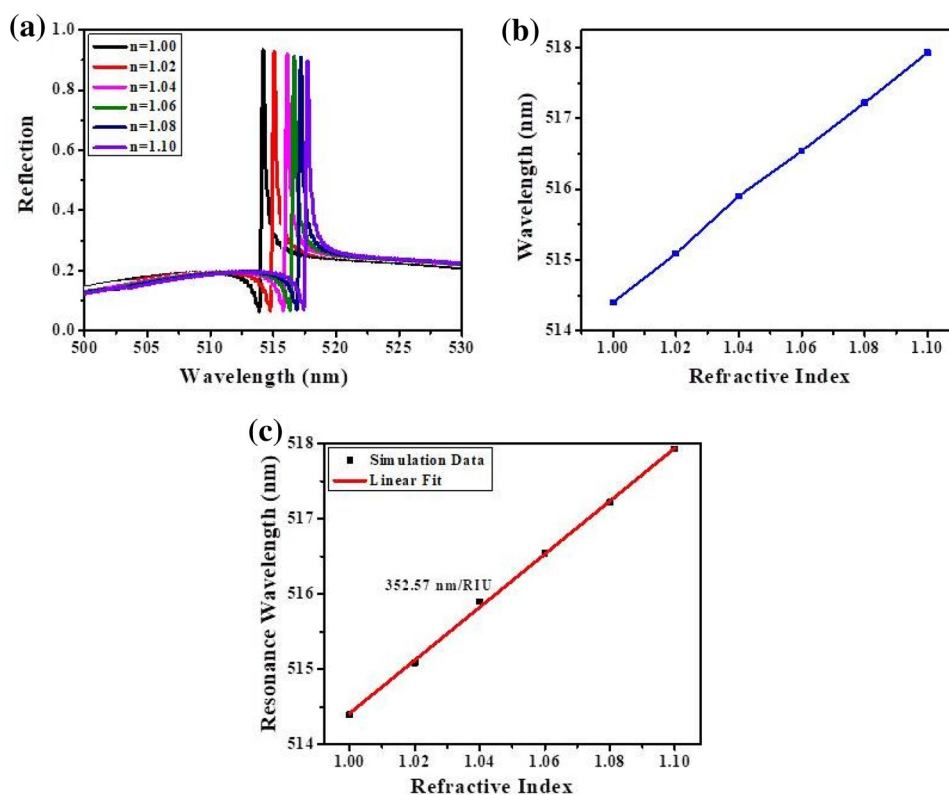
changes linearly with a minor variations in RI of the background medium. Hence, we proposed a sensitivity ($S = d\lambda / dn$) that defines the resonant peak wavelength variations per refractive index unit [29]. In this simulation, peak shift of wavelength from 514 nm to516nm nm represent by small variations of dn = 0.02. Sensitivity as high as 352.57 is obtained by using this formula. In accordance to Fig. 2c, peak is linear fitted to obtain sensitivity value. The related FOM, describes as the ratio of sensitivity and the resonance linewidth to illustrate the sensing abilities of 1D structure, which stated as FOM = S/λ. Here, λ is the resonance line width.

Extreme narrow FWHM as slight as 0.25 nm may attained by simulating GMR-based structure. Hence, the simulated structure suggested in this paper can attain the value of FOM as great as 1176. By varying the parameters of the nanostructure a lower FWHM of GMR can be achieved, which will advance the sensing ability by showing higher FOM values. It will be discussed in later sections.

Ensuing previous hypothetical methodology, we provide a assessable explanation of the peak alteration with variations of the RI [39]. The GMR positions calculated in Fig. 2c, d, are in decent arrangement with our simulated data, that approves the linear dependency of resonant peak change on the variation of the RI value.

To simplify complete discussion on the recommended configuration, and to improve its result, all parameters, with

Λ, angle, and h had been studied in facet. GMR is normally sensitive to the incident angle [40]. We observe the spectral position of the particular resonances is quietly adjustable by varying grating configuration and is much acute to gratings configuration. It is revealed such geometries produce entire energy transfer with stable line shapes and swiftly narrow filter line widths. To achieve highly capable sensor, a spatial-frequency grating is preferred to avoid the larger diffractive orders from the transmission.TiO$_2$ GMR grating simulated on the glass substrate, which also shows good property TM non polarized sensor and the ability of low-cost mass reproduction of the functional device.

Grating with diverse dimensions and periods, which attempt to control spectral aspects like the FWHM of the reflectivity resonance or GMR spectral location, bandwidth, and sensitivity. To advance insights toward the reactivity of the resonance through altering grating parameters, we managed FDTD computation in which we exclusively used different parameters P, angle as well as h although keeping the other parameters unchanged.

The different values of the period have a specific effect on resonance positions, but relatively do not alter the spectral thickness of the filter. The spectral width is generally determined through the grating thickness; this is due to the resonant reflection that appears at the compact of grating and substrate. Compared to the result exhibited in Fig. 3, we observed that decrease in grating height which considerably

Fig. 3 **a** Simulated reflectance spectra as a function of height **b** Graph between FWHM and the height **c** Relationship between FOM and the height
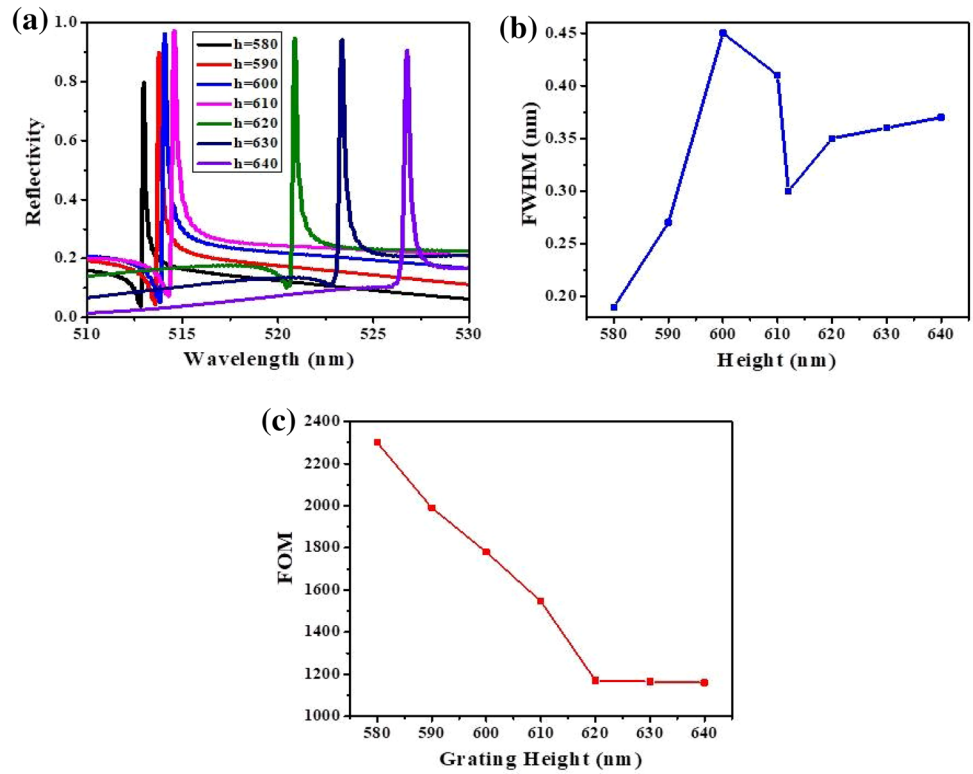
enhances the abilities of the simulated 1D structure, when $P = 500$ nm, $f = 0.685$ and $\theta = 0°$. The reflectivity spectrum

of our proposed RI sensor has been observed with various grating depths varying from 580 to 640 nm in Fig. 4a.

Fig. 4 **a** Simulated reflectance spectra as a function of period **b** Graph between FWHM and the period **c** Relationship between FOM and the period
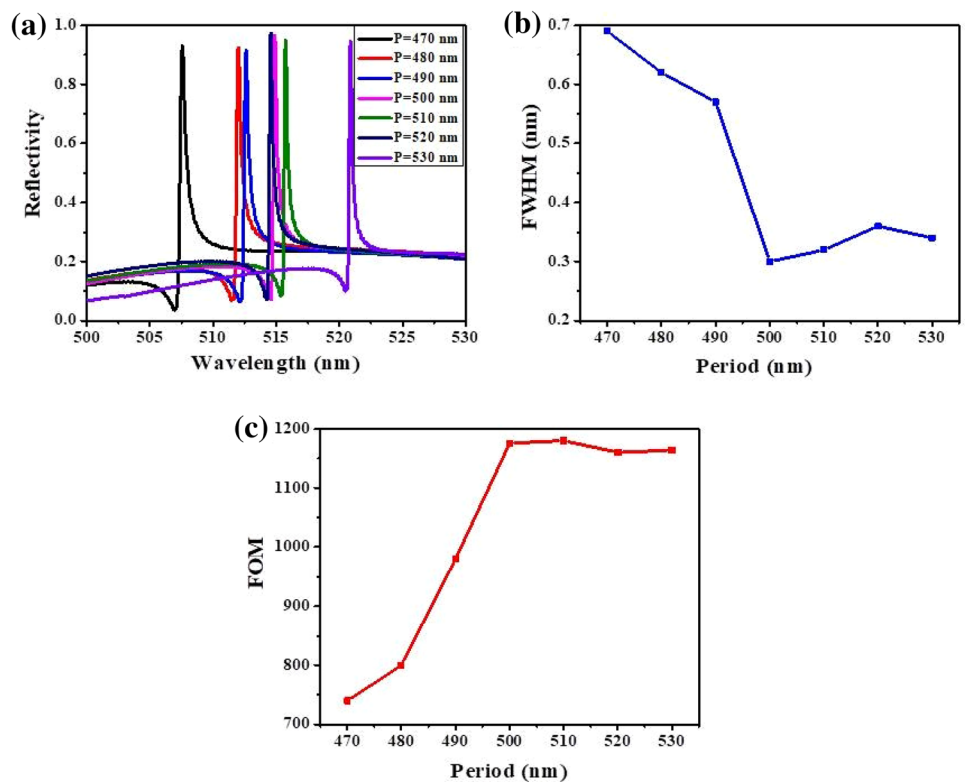
Both major properties are obvious: (i) the peak location of the resonant wavelength changes which shows red -shift from 514 nm with grating height $h = 600$ to 620 nm and (ii) the FWHM increases considerably as the grating height decreases. It shows that a decreased h gives a small peak value and large propagation loss for TM mode. While by the varying value of h, the small change was noticed in peak deviation. Moreover, the reflection of TE/TM is very close to mode overlap. As h varies from 580 to 600 nm, the midpoints of wavelength deviation towards the lower wavelength because of increased momentary coupling among both resonant modes. Tunable resonance on the linked gratings can be used to handle the swapping intensity. Thus, we set $h = 612$ nm to equate the linked coefficient and transformation loss. We deduced the FWHM as a function of grating depth, shown in Fig. 4b. The FWHM increases with enhance in the grating thickness; moreover, the full-width half-maximum reduces with the reduction in the grating thickness. So, the required FWHM may attain by changing the grating thickness. We can observe that the FWHM reduces from ~ 0.33 nm to ~ 0.19 nm for grating depth $h = 580$ nm.

To estimate the sensing competency, we varies the RI of the background medium nc from 1 to 1.01 to evaluate the sensitivity and FOM of our simulated GMR-device with changed grating height. The resulted Figure of merit values according to different grating height are given in Fig. 4c, which shows the FOM of our simulated RI sensor retains up to 2400 and increases fastly after the grating depth surpasses to decreases. Narrow linewidth for small grating depth shows high FOM, which is because of the interaction among drippy waveguide mode as well as the infinitely transmitting diffracted fields. Moreover, we discover the grating height value of 580 nm exceeds the FOM with narrow linewidth peak approaching to ~ 0.19 nm. Hence, suitable selecting of grating height offers a proficient method to efficiently lessen resonant linewidth and therefore enhance the behavior of our RI sensor.

Period is the main parameter, which effects sensitivity and shifts GMR peak wavelength. Modification in the repetition affects GMR which causes peak change and influences the waveguide modes in figure below. The gap among gratings plays a crucial role to obtain the desired wavelength. Increase in spacing between gratings causes peak deviation because it changes the desired geometry of the structure. Spacing between gratings plays an important role because it supports the guided-mode resonance between them.

Relevant papers exposes that a higher period cause increase in peak wavelength and higher sensitivity values [41, 42], although it is uncertain if Λ will effect linewidth or the consistent figure of merit. To understand FOM, Period changing from 470 to 530 nm, were selected to calculate the point at which there is a lesser resonant line width as well as higher sensitivity being TM polarization as shown in

Fig. 4a. Sensitivity having direct relationship with Λ as well as the resonant line width firstly increased, and then reduced in symmetric configuration as shown in Fig. 4b. Generally FOM improved as Λ increased, in Fig. 4c, and considering these outcomes, if the purpose was to attain an excellent GMR sensor, a larger Λ was an actual method, using the suggested structure. To fit our consequent simulations, a 500-nm Λ had been used when we considered the effects of other factors. We chose $P = 500$ nm to examine resonance at choose wavelength. This investigation indicates that grating spacing has the most dominant grip in regulating the peak position of grating mode resonance. The noticed resonance coincides with the zero-order mode. Just as the wavelength about the incident transporting wave reduces, further greater order modes turn into accessible, which propose further resonances. Focusing on sensing ability, an effect of the grating period and change in height had been found as a mark to achieve an improved sensor.

The resonance aspect that appears in our one-dimensional dielectric GRATING produces using a grating mode resonance, in that incident light sets into guided modes of grating due to the phase identical position that grants for an incident wave toward a guided mode. To explain the outcome of incident angle, Fig. 5 reveals a graph among illumination angle and the related reflectivity spectra provoked by FDTD simulations.

Figure 5 exhibits the FDTD reflectivity spectrum for a TiO_2 grating with $w = 343$ nm, $P = 500$ nm, and $h = 612$ nm with different incident light angles which diverge from 0° to 40° for p-polarization. Using this operation for each incident angle grants us to precisely find out the adequate band and conclude the role of the GMR usage. Under natural incidence of light, grating have a bandgap mode over the noticed frequency of reflectivity peak. In the meantime, detected around-unity reflections can occur to be grating band gap
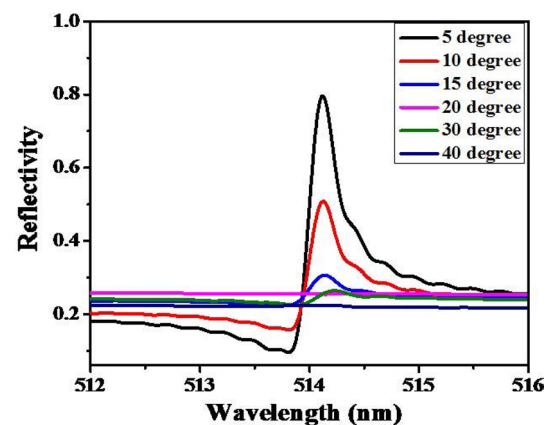

Fig. 5 FDTD simulations of reflectivity spectra for TiO_2 GRATING under an incident illumination angle that varies from 0° to 40° in 5° increments for TM polarization

Table 1 Comparison of GMR and other optical sensor

Types of Sensors	FWHM(nm)	S(nm/RIU)	FOM	Ref
1D Ti0$_2$ Grating	0.3	352.7	1176	This work
Ultralow RI substrate GMR device	~ 11	502	50	[43]
One-dimensional all-dielectric nanoslit array	0.3	301	1190	[44]
Metal layer assisted GMR device	~ 15	376.78	25	[45]
Low-index cavity GMR device	9.3	181.9	20	[46]
Chirped grating GMR device	12	160	13	[47]
Low-index porous dielectric GMR	3.5	302.22	86	[7]
Typical GMR device	5.2	112.4	22	[48]
Typical GMR device	4.33	186.66	43	[41]
All-polymer GMR device	0.9	31	34	[48]
PHC cavity device	0.085	94.5	1100	[31]
Nanoring Resonator	…….	2080	29.92	[49]
Parallel planar waveguide gratings	…….	497.83	551	[50]
Single-layer guided-mode resonance	7.28	229.43	31.52	[51]
SGMR (TM)	14.01	125.89	8.99	[51]

implement in the background of the periodic scheme, maybe this is not the scenario, as the positions of the computed GMRs are very narrow to extend as well as reflection peaks certainly follow the ordinary incident illumination comparatively than another typical incidence are studied. Moreover, the noticed reflection coincides with specular transportation, or 0th-order diffraction, in a sub-wavelength pattern. The optical region damped rapidly when TM mode is inserted by using a higher-order value of angle based on the reflection of the PG as well as SPPs stimulation. The 1st-order diffraction point appears at 514 nm. These findings show that it is feasible to efficiently restraint the spectral quality of the grating mode resonance, granting for important structure affability in designing a sensor.

For the TM approach, α has a response on the reflection due to a small variation of angle that can start a massive disruption in SPPs stimulated through TM mode. Thus, in the simulation kept $\alpha = 0°$ can generate the better sensing properties. As the performance of the sensor has been greatly affected with the PG structure parameters because of the SPPs effect, we modified gratings thickness h, incident angle, and period.TM mode gains a broad SSPS mode, as well as light, is firmly confined, making it further suitable to attain better performance.

Sensing properties for sensitivity (S) had been studied by using the same parametric study. It is observed that the sensitivity of refractive index sensor became higher by increasing Λ and decreasing h. It also decreases while the incidence angle becomes higher. Figure 4c reveals that the FOM rises with the decreased height (because of increasing sensitivity and reducing FWHM). Even with the substantial proliferation in sensitivity with Λ, the figure of merit value declines under the effect of the resonance broadening. As predictable from the result of the incidence angle on the

Q-factor, the FOM experiences a sharp decline as soon as the symmetry has been broken by differing from the normal incidence. Therefore, we can determine that high sensing results are reached for these structures with the 2D-grating geometries. It is noticeable that the sensitivity of the aforementioned structure is smaller than the diverged resonant mode design based on the metal grating and the one-layer GMR system. These techniques substantially magnify the electric field intensity in the sensing area, and therefore the sensitivity improvement is evident. Though, the complex design or the firm structural parameter settings with small resistance making the absolute performance is efficiently affected through the fabrication faults. On the contradiction, our model delivers a more quiet and efficient approach to achieve good performance grating-based sensor. Also, we would like to affirm that, the recommended simple, steady, good performance GMR sensor is significantly suitable for large-throughput industrial level production and gravel the way for point-of-care usages. The simulated GMR design is favorable for future possible applications at visible wavelength. The comparison of this study with literature is given in Table 1.

4 Conclusion

We illustrated a TiO$_2$ -based refractive index sensor at visible wavelengths. Since the execution of the GMR sensor is highly affected by the structure specifications because of the effect of SPPs, we modified the gratings height, width, period, and incident angle. By changing the parameters, we can efficiently advance the performance of our simulated refractive index sensor. Through adjusting the geometric factors of the dielectric grating, we attain a high

FOM above 1100 with narrow linewidth down to 0.3 nm due to the interference among leaky waveguide approach and the eternally spreading diffracted fields. Such a simply simulated all-dielectric RI sensor based on GMR is estimated to recognize broadband sensing with extraordinary performance.

Declarations

Conflict of interest There are no conflicts to declare.

References

1. Liu, Z., Tibuleac, S., Shin, D., Young, P., Magnusson, R.: High-efficiency guided mode resonance filter. Opt. Lett. **19**, 1556–1558 (1998)
2. Mazulquim, D., Lee, K., Yoon, W., Muniz, L., Borges, H., Neto, L., Magnusson, R.: Efficient band-pass color filters enabled by resonant modes and plasmons near the Rayleigh anomaly. Opt. Express **22**, 30843 (2014)
3. Fang, C., Dai, V., Li, Z., Zahid, A., Wang, V., Sheng, V., Zhang, D.: Tunable guided-mode resonance filter with a gradient grating period fabricated by casting a stretched PDMS grating wedge. Opt. Lett. **41**, 5302–5305 (2016)
4. Mizutani, A., Kikuta, H., Iwata, K.: Numerical study on an asymmetric guided-mode resonant grating with a Kerr medium for optical switching. J. Opt. Soc. Am. A **22**, 355–360 (2005)
5. Wawro, D., Tibuleac, S., Magnusson, R., Liu, H.: Optical fiber end face biosensor based on resonances in dielectric waveguide gratings. Proc. SPIE **3911**, 86–94 (2000)
6. Kim, W., Kim, B., Kim, A., Huh, C., Ah, C., Kim, K., Hong, J., Park, S., Song, S., Song, J., Sung, G.: Response to cardiac markers in human serum analyzed by guided-mode resonance biosensor. Anal. Chem. **82**, 9686–9693 (2010)
7. Block, I., Chan, L., Cunningham, B.: Photonic crystal optical biosensor incorporating structured low-index porous dielectric. Sens. Actuators B **120**, 187–193 (2006)
8. Sancho, F., Avella, O., Carrascosa, J., Fernandez, E., Brun, E., Maquieira, A.: Disk-based one-dimensional photonic crystal slabs for label-free immunosensin. Biosens. Bioelectron. **126**, 315–323 (2010)
9. Triggs, G., Wang, Y., Reardon, C., Fischer, M., Evans, G., Krauss, T.: Chirped guided-mode resonance biosensor. Optica **4**, 229–234 (2017)
10. Magnusson, R., Wang, S.: New principle for optical filters. Appl. Phys. Lett. **61**, 1022 (1992)
11. Abdallah, M., Buchanan, J., Lee, K., Wenner, B., Allen, J., Allen, M., Gimlin, S., Wawro, D., Magnusson, R.: Quantification of neuropeptide y with picomolar sensitivity enabled by guided-mode resonance biosensors. Sensors **20**, 126 (2020)
12. Cunningham, B., Li, P., Lin, B., Pepper, J.: A plastic colorimetric resonant optical biosensor for multiparallel detection of label-free biochemical interactions. Sens. Actuators B Chem. **81**, 316–332 (2002)
13. Guo, L., Wang, Q., Huang, Y., Zhang, D.: Portable organic gas detection sensor based on the effect of guided-mode resonance. AIP Adv. **7**, 015031 (2017)
14. Sahoo, P., Sarkar, S., Joseph, J.: High sensitivity guided-mode-resonance optical sensor employing phase detection. Sci. Rep. **7**, 7607 (2017)
15. Zhu, Y., Zhang, H., Li, D., Zhang, Z., Zhang, S., Yi, J., Wang, W.: Magnetic plasmons in a simple metallic nanogroove array for refractive index sensing. Opt. Express **26**, 9148–9154 (2018)
16. Liu, Y., Ma, Y.: One-dimensional plasmonic sensor. Front. Phys. **8**, 312 (2020)
17. Bagheri, F., Soroosh, M., Haddadan, F., Seifi-Kavian, Y.: Design and simulation of a compact graphene-based plasmonic D flip-flop. Laser Technol. **155**, 108436 (2022)
18. Haddadan, F., Soroosh, M.: Design and simulation of a subwavelength 4-to-2 graphene-based plasmonic priority encoder. Laser Technol. **157**, 108680 (2023)
19. Stocker, G., Spettel, J., Dao, T., Tortschanoff, A., Jannesari, R., Puhringer, G., Saedi, P., Dubois, F., Fleury, C., Consani, C., Grille, T., Jackoby, B.: Ultra-narrow SPP generation from Ag grating. Sensors **21**, 6993 (2021)
20. Haddadan, F., Soroosh, M., Alaei-Sheini, N.: Cross-talk reduction in a graphene-based ultra-compact plasmonic encoder using an Au nano-ridge on a silicon substrate. Appl. Opt. **61**, 3209–3217 (2022)
21. Verellen, N., Van Dorpe, P., Huang, C., Lodewijks, K., Vandenbosch, G., Lagae, L., Moshchalkov, V.: Plasmon line shaping using nanocrosses for high sensitivity localized surface plasmon resonance sensing. Nano Lett. **11**, 391–397 (2011)
22. Lassiter, J., Sobhani, H., Fan, J., Kundu, J., Capasso, F., Nordlander, P., Halas, N.: Fano resonances in plasmonic nanoclusters: geometrical and chemical tunability. Nano Lett. **10**, 3184–3189 (2010)
23. Auguie, B., Barnes, W.L.: Collective resonances in gold nanoparticle arrays. Phys. Rev. Lett. **101**, 143902 (2008)
24. Hicks, E., Zou, S., Schatz, G., Spears, K., Van, R., Duyne, L., Gunnarsson, T., Rindzevicius, B., Kasemo, M.: Controlling plasmon line shapes through diffractive coupling in linear arrays of cylindrical nanoparticles fabricated by electron beam lithography. Nano Lett. **5**, 1065–1070 (2005)
25. Vecchi, G., Giannini, V., Rivas, J.G.: Surface modes in plasmonic crystals induced by diffractive coupling of nanoantennas. Phys. Rev. B **80**, 201401 (2009)
26. Haddadan, F., Soroosh, M., Alaei-Sheini, N.: Cross-talk reduction in a graphene-based ultra-compact plasmonic encoder using an Au nano-ridge on a silicon substrate. Appl. Opt. **59**, 2179–2185 (2020)
27. Sang, T., Wang, Z., Zhu, J., Wang, L., Wu, Y., Chen, L.: Linewidth properties of double-layer surfacerelief resonant brewster filters with equal refractive index. Opt. Express **15**, 9659–9665 (2007)
28. Wang, Z., Sang, T., Zhu, J., Wang, L., Wu, Y., Chen, L.: Double-layer resonant brewster filters consisting of a homogeneous layer and a grating with equal refractive index. Appl. Phys. Lett. **89**, 241119 (2006)
29. Ju, J., Han, Y., Kim, S.: Design optimization of structural parameters for highly sensitive photonic crystal label-free biosensors. Sensors **13**, 3232–3241 (2013)
30. Pitruzzello, G., Krauss, T.: Photonic crystal resonances for sensing and imaging. J. Opt. **20**, 073004 (2018)
31. Liu, Y., Wang, S., Zhao, D., Zhou, W., Sun, Y.: High quality factor photonic crystal filter at $k \approx 0$ and its application for refractive index sensing. Opt. Express **25**, 10536–10545 (2017)
32. Ge, C., Lu, M., George, S., Flood, T., Wagner, C., Zheng, J., Pokhriyal, A., Eden, J., Hergenrother, P., Cunningham, B.: External cavity laser biosensor. Lab. Chip. **13**, 1247 (2013)
33. Fan, S., Joannopoulos, J.: Analysis of guided resonance in photonic crystal slabs. Phys. Rev. B **65**, 235112 (2002)
34. Fan, S., Suh, W., Joannopoulos, J.: Temporal coupled-mode theory for the Fano resonance in optical resonators. J. Opt. Soc. Am. A **20**, 569–572 (2003)
35. Chang-Hasnain, C., Yang, W.: High-contrast gratings for integrated optoelectronics. Adv. Opt. Photonics **4**, 379–440 (2012)

36. Lalanne, P., Hugonin, J., Chavel, P.: Optical properties of deep lamellar gratings: a coupled bloch-mode insight. J. Lightwave Thechnol. **24**, 2442–2449 (2006)

37. Barillaro, G., Merlo, S., Surdo, S., Strambini, L., Carpignano, F.: Integrated optofluidic microsystem based on vertical high-order one-dimensional silicon photonic crystals. Microfluid. Nanofluidic. **12**, 545–552 (2012)

38. Peters, D., Kemme, S., Hadley, G.: Effect of finite grating, waveguide width, and end-facet geometry on resonant subwavelength grating reflectivity. J. Opt. Soc. Am. A **21**, 981–987 (2004)

39. Wang, S., Magnusson, R.: Theory and applications of guided-mode resonance filters. Appl. Opt. **32**, 2606–2613 (1993)

40. Piper, J., Fan, S.: Total Absorption in a graphene monolayer in the optical regime by critical coupling with a photonic crystal guided resonance. ACS Photonics **1**, 347–353 (2014)

41. Tsai, M., Hsiung, C., Chen, Y., Hsu, H., Hsieh, P.: Real-time CRP detection from whole blood using micropost-embedded microfluidic chip incorporated with label-free biosensor. Analyst **143**, 503–510 (2018)

42. Lin, S., Wang, C., Tsai, Y., Ding, T., Yang, T., Chen, W., Yeh, S., Chang, J.: A model for fast predicting and optimizing the sensitivity of surface-relief guided mode resonance sensors. Sens. Actuators B Chem. **176**, 1197–1203 (2013)

43. Wan, Y., Krueger, N., Ocier, C., Su, P., Braun, P., Cunningham, B.: Resonant mode engineering of photonic crystal sensors clad with ultralow refractive index porous silicon dioxide. Adv. Opt. Mater. **5**, 1700605 (2017)

44. Lan, G.: High- performance refractive index sensor based on guided mode resonances in all-dielectric nano-slit array. Phys. Lett. A **1**, 057 (2019)

45. Lin, S., Wang, C., Ding, T., Tsai, Y., Yang, T.H., Chen, W.Y., Chang, J.Y.: Sensitive metal layer assisted guided mode resonance biosensor with a spectrum inversed response and strong asymmetric resonance field distribution. Opt. Express **20**, 14584–14595 (2012)

46. Ku, Y., Li, H., Hsieh, W., Chau, L., Chang, G.: Enhanced sensitivity in injection-molded guided-mode-resonance sensors via low-index cavity layers. Opt. Express **23**, 14850–14859 (2015)

47. Boonruang, S., Mohammed, W.: Multiwavelength guided mode resonance sensor array. Appl. Phys. Express **8**, 092004 (2015)

48. Tu, Y., Tsai, M., Lee, I., Hsu, H., Huang, C.: Integration of a guided-mode resonance filter with microposts for in-cell protein detection. Analyst **141**, 4189–4195 (2016)

49. Chao, C., Chau, Y., Huang, H., Kumara, N., Kooh, M., Lim, C., Chiang, H.: Highly sensitive and tunable plasmonic sensor based on a nanoring resonator with silver nanorods. Nanomaterials **10**, 1399 (2020)

50. Lu, X., Zheng, G., Zhou, P.: High performance refractive index sensor with stacked two-layer resonant waveguide grating. Results Phys. **12**, 759–765 (2019)

51. Qian, L., Wang, K., Han, C., Yan, C.: Enhanced sensing ability in a single-layer guided-mode resonant optical biosensor with deep grating. Opt. Commun. **452**, 273–280 (2019)